

The nature of dark matter from the global high redshift HI 21 cm signal

M. Valdés^{1,3*}, C. Evoli^{2,1}, A. Mesinger¹, A. Ferrara^{1,3} & N. Yoshida^{4,3}

¹ *Scuola Normale Superiore, Piazza dei Cavalieri 7, 56126 Pisa, Italy*

² *II. Institut für Theoretische Physik, Universität Hamburg, Luruper Chaussee 149, 22761 Hamburg, Germany*

³ *Kavli IPMU, University of Tokyo, 5-1-5 Kashiwanoha, Kashiwa, Chiba 277-8568, Japan*

⁴ *Department of Physics, University of Tokyo, 3-7-3 Hongo, Bunkyo-ku, Tokyo 113-0033, Japan*

23 October 2021

ABSTRACT

We study the imprint of dark matter (DM) annihilation on the global 21 cm signal from the Dark Ages to Cosmic Reionization. Motivated by recent observations, we focus on three DM candidates: (i) a 10 GeV Bino-like neutralino (ii) a 200 GeV Wino and (iii) a 1 TeV heavier particle annihilating into leptons. For each DM candidate we assume two values for the thermally averaged annihilation cross section $\langle\sigma v\rangle$, the standard thermal value $\langle\sigma v\rangle_{th} = 3 \times 10^{-26} \text{cm}^3 \text{s}^{-1}$ and the maximum value allowed by WMAP7 data, $\langle\sigma v\rangle_{max}$. We include the enhancement of DM annihilations due to collapsed structures, detailed estimates of energy deposition into the intergalactic medium (IGM), as well realistic prescriptions for astrophysical sources of UV and X-ray radiation. In these models, the additional heat input from DM annihilation suppresses the mean 21cm brightness temperature offset by $\delta T_b \sim \text{few} - 100 \text{ mK}$. In particular, the very deep $\delta T_b \sim -150 \text{ mK}$ absorption feature at $\sim 20 \lesssim z \lesssim 25$ predicted by popular models of the first galaxies is considerably reduced or totally erased by some of the considered DM candidates. Such an enhancement in IGM heating could come from either DM annihilations or a stronger-than-expected astrophysical component (i.e. abundant early X-ray sources). However, we find that the two signatures are not degenerate, since the DM heating is dominated by halos several orders of magnitude smaller than those hosting galaxies, whose fractional abundance evolves more slowly resulting in a smaller gradient: $d\delta T_b/d\nu \lesssim 4 \text{ mK/MHz}$ in the range $\nu \sim 60 - 80 \text{ MHz}$. The detection of such signals by future radio telescopes would be clear evidence of DM energy injection at high-redshifts.

Key words: intergalactic medium - cosmology: theory - diffuse radiation - dark matter

1 INTRODUCTION

In the framework of the successful Λ CDM cosmology theory only $\sim 5 \%$ of the current energy content of the Universe is made of visible matter, while the rest is divided into two *dark* components, 73 % in the form of the so called Dark Energy, with the remaining 22 % accounted for by Dark Matter (DM) which only interacts with baryons through gravity (Komatsu et al. 2009). The existence of DM seems to be indirectly confirmed by a large set of observations (even though it is conceivable that in the future a new theory of gravity could do without DM), however its nature remains unknown. The accuracy of Λ CDM in explaining the evolution of the Universe is one of the major successes of modern

cosmology; however the question of what makes up over 95 % of the Universe is still open.

A huge effort has been made in the past decades to detect DM directly and indirectly. Currently, the best we can do is to place constraints on the properties (e.g. mass, annihilating cross section, decay rate) of some of the proposed DM candidates, thanks mostly to recent observations. We will focus here on Weakly Interacting Massive Particles (WIMPs) that are among the most popular DM candidates since their existence and properties are predicted by several extensions of the Standard Model of particle physics.

WIMPs have a small but non negligible interaction cross-section with ordinary matter and therefore in principle they can be directly detected via elastic collision with the nuclei of terrestrial targets. Several recent experiments such as DAMA/LIBRA, DAMA/NaI, CDMS-II, EDELWEISS-II,

* E-mail: marcos.valdes@sns.it

CoGeNT, XENON100 have attempted such detection (see e.g. Bernabei et al. 2004, 2008, 2010; Aalseth et al. 2011a,b; Aprile et al. 2011; CDMS II Collaboration et al. 2010; Armengaud et al. 2010). Promising results came from CoGeNT, which reported about a hundred events exceeding the expected background, possibly originated from the nuclear recoil by scattering from DM particles of mass $M_\chi \lesssim 10$ GeV. A light WIMP with similar mass is also favored by the recent DAMA/LIBRA annual modulation signal (Bernabei et al. 2010; Aalseth et al. 2011a,b).

Astrophysical observations in the X-ray and Gamma radiation bands have also been used to indirectly detect a DM generated signal. A lot of excitement followed the recent detection by the PAMELA, ATIC, FERMI-LAT and HESS experiments of an excess in the electron/positron cosmic ray energy spectrum, which could be explained by annihilating DM with mass of order of 1 TeV (see e.g. Cirelli, Franceschini & Strumia 2008; Liu et al. 2010; Berg et al. 2009; Hooper & Tait 2009; Chen, Takahashi & Yanagida 2009; Abdo et al. 2010). The results appear to be far from conclusive due to the difficulties in properly modeling the cosmic ray energy spectrum and because other astrophysical sources such as pulsars could be responsible for the signal (see e.g. di Bernardo et al. 2011; Profumo 2012).

Another promising observational window for the indirect search of DM will be available in the near future when next generation radio interferometers such as the Low frequency Array (LOFAR¹), the 21 Centimeter Array (21CMA²), the Murchison Widefield Array (MWA³) and the Square Kilometer Array (SKA⁴). These large interferometers will be able to map at arcminute scales the redshifted 21 cm line corresponding to the hyperfine triplet-singlet line transition of the ground level neutral hydrogen (HI) at $z > 6$, i.e. during the Epoch of Reionization (EoR) and possibly well into the so called Cosmic Dark Ages of the Universe (see e.g. Peterson, Pen & Wu 2005; Bowman, Morales & Hewitt 2006; Kassim et al. 2004; Wyithe, Loeb & Barnes 2005).

The global sky-averaged 21 cm signal could potentially be measured as a function of frequency even by single dipoles: this is the main scientific aim of current instruments such as the Experiment to Detect the Reionization Step (EDGES), while more advanced ones such as the Large-aperture Experiment to Detect the Dark Ages (LEDA⁵) and the Dark Ages Radio Experiment (DARE⁶), a lunar orbiting dipole experiment, are planned for construction (see e.g. Bowman & Rogers 2010; Greenhill & Bernardi 2012; Burns et al. 2012).

Any release of energy from DM - for instance, as is the case considered in this work, through annihilations - would be in part absorbed by the intergalactic medium (IGM) as heat and ionization. If this occurred before the first astrophysical sources ($z \gtrsim 30$), it would produce a deviation from the theoretically well established thermal and ionization history (see e.g.

Chen & Kamionkowski 2004; Mapelli, Ferrara & Pierpaoli 2006; Cirelli, Iocco & Panci 2009) and could alter significantly the HI 21 cm signal (see e.g. Shchekinov & Vasiliev 2007; Furlanetto, Oh & Pierpaoli 2006; Valdés et al. 2007; Natarajan & Schwarz 2009; Galli et al. 2011; Finkbeiner et al. 2012). If the DM energy injection occurred after the first astrophysical sources ($z \lesssim 30$), the deviation could be stronger and easier to observe, but would have to be disentangled from astrophysical uncertainties concerning the first galaxies. There are enormous observational challenges in detecting the 21 cm signal at $z \gtrsim 30$, and such observations may be decades away from our current technological level. For this reason, we focus on the DM signal at lower redshift, after stars and galaxies started forming, and look for strategies to separate the DM signal from that of astrophysical sources.

We investigate the effects produced on the HI 21 cm signal by three DM candidates: (i) a 10 GeV Bino-like neutralino (ii) a 200 GeV Wino and (iii) a 1 TeV heavier particle annihilating into leptons. These candidates have been recently proposed to explain the aforementioned indirect/direct hints of DM detection. We allow the annihilation cross-section to be in a range which is compatible with CMB observations. For the first time we compute the 21 cm DM signal at $z \lesssim 30$ in a self consistent scenario that includes a realistic prescription for the formation of astrophysical sources of UV and X-ray radiation.

The details of the energy deposition into the IGM from DM annihilations are an essential ingredient to compute the HI 21 cm signal. In Evoli et al. (2012b) we have studied the cascade produced by the products of DM annihilations for the three considered DM candidates: this allows us to discuss the impact of DM annihilations in a physically consistent way and to assess the observability of the chosen DM candidates with HI 21 cm observations in the near future.

The rest of the paper is organized as follows. In Sec. 2 we briefly introduce the DM candidates which we study; in Sec. 3 we explain in detail the method that we follow to compute the 21 cm DM signal. In Sec. 4 we present the results of our calculations, and in Sec. 5 we discuss the results and draw our conclusions.

2 DARK MATTER MODELS

In this Section we briefly introduce our DM models of choice. For a more detailed discussion of such DM particle candidates we refer the reader to Evoli et al. (2012a), where they are described extensively. We select three sample cases which have been recently investigated in connection with hints of DM signals in either direct and indirect search experiments. These sample cases are also representative of three different WIMP mass regimes, ranging from fairly light models to multi-TeV DM, and of three different kinds of annihilation channels.

Wino: We consider a pure Wino within the Minimal Supersymmetric extension to the Standard Model (MSSM). The recent interest in this model has been stimulated, besides its peculiar signatures at the LHC (Bertone et al. 2012), by the claim (Grajek et al. 2009; Kane, Lu & Watson 2009) that a Wino with mass of about 200 GeV can explain the rise detected by PAMELA in the positron fraction.

¹ <http://www.lofar.org/>

² <http://21cma.bao.ac.cn/>

³ <http://www.mwatelescope.org/>

⁴ <http://www.skatelescope.org/>

⁵ <http://www.cfa.harvard.edu/LEDA/>

⁶ <http://lunar.colorado.edu/dare/mission.html>

Bino: We consider the $\bar{b}b$ case with mass of 10 GeV to model a strong coupling with quarks as suggested by recent results of direct detection experiments (e.g. CDMS, DAMA).

Leptophilic: Again motivated by the PAMELA positron excess, and possibly in connection with the local all-electron (namely electrons plus positrons) flux measured by Fermi and HESS, several analyses have considered the possibility of very heavy dark matter WIMPs, with masses up to several TeV and very large pair annihilation cross section (see e.g. Cirelli et al. 2009; Bergström, Edsjö & Zaharijas 2009). The results of such studies are that, to account for the electron/positron component without violating the anti-proton bounds, dark matter needs to be *leptophilic*, i.e. the final products of the annihilation being dominantly leptons, most likely a combination of e^+e^- and $\mu^+\mu^-$. It has been recently pointed out (Ciafaloni et al. 2011) that for very heavy WIMPs the radiative emission of soft electroweak gauge bosons is crucial to model the high-energy spectrum.

3 METHOD

We first constrain the properties of our DM candidates from CMB data. This allows us to associate to each particle a range of allowed values for the annihilation cross section $\langle\sigma v\rangle$. We then use the fractional energy depositions from MEDEA2 (Evoli et al. 2012b) and the galactic radiation fields from 21cmFAST (Mesinger, Furlanetto & Cen 2011) in order to compute the thermal and ionization evolution of the IGM and the associated global 21cm signal. We describe each of these steps in turn.

3.1 DM heating

Including the formation of substructures at redshift $\lesssim 50$ naturally enhances the effects of DM annihilations: while they do not dramatically impact the global reionization history (Cirelli, Iocco & Panci 2009) the increased energy injection could alter predictions of the observable 21 cm signal by heating the IGM. The total energy release by DM annihilations per unit volume is given by (see e.g. Cirelli, Iocco & Panci 2009; Chluba 2010):

$$\frac{dE_\chi}{dt} = 2M_\chi c^2 \langle\sigma v\rangle n_\chi^2 (1 + B(z)), \quad (1)$$

where $\langle\sigma v\rangle$ is the thermally averaged annihilation cross section, M_χ is the DM particle mass and $n_\chi = n_{0,\chi}(1+z)^3$ is the number density of DM particles and anti-particles with present day value:

$$n_{0,\chi} = 1.2 \times 10^{-8} \text{ cm}^{-3} \left(\frac{\Omega_\chi h^2}{0.11} \right) \left(\frac{M_\chi c^2}{100 \text{ GeV}} \right)^{-1}. \quad (2)$$

The term $B(z)$ defines the effective averaged DM density resulting from structure formation and can be written as:

$$B(z) = \frac{\Delta_{\text{vir}}(z)}{3\rho_c \Omega_M} \int_{M_{\text{min}}}^\infty dM M \frac{dn}{dM}(z, M) F(M, z) \quad (3)$$

where dn/dM is the halo mass function obtained adopting the Press-Schechter formalism (Press & Schechter 1974) and $F(M, z)$ is the concentration function depending on the distribution of DM inside halos, a function that peaks typically for sub-halo masses $M_{\text{sh}} \sim 1 \text{ M}_\odot$ at $z = 20$ (see

Fig. 7; we refer the reader to Cirelli, Iocco & Panci 2009 for details)⁷. We use here a prescription for the effect of substructures and consider a minimum mass for primordial proto-haloes of $M_{\text{min}} = 10^{-6} \text{ M}_\odot$ for the 10 GeV Bino, and $M_{\text{min}} = 10^{-9} \text{ M}_\odot$ for the other two more massive candidates. This choice is motivated by recent calculations of the exponential cutoff mass in the power spectrum as a function of neutralino mass, resulting from free-streaming of the DM particles after the kinetic decoupling (see e.g. Bringmann 2009; van den Aarssen, Bringmann & Goedecke 2012).

Recent works (e.g. Slatyer, Padmanabhan & Finkbeiner 2009; Galli et al. 2009) have investigated the possible role of Sommerfeld enhancements due to which $\langle\sigma v\rangle$ can be considerably boosted and becomes a function of redshift. We choose not to make assumptions on the physical processes that could boost $\langle\sigma v\rangle$ and treat it as a parameter constrained by CMB observations.

We covered until now the energy *production* by DM annihilations. The most relevant quantity for our purposes is however the energy *deposition* into the IGM. Only a small fraction of the energy released by DM annihilations is finally deposited into the IGM in the form of heat, excitations and ionizations either of hydrogen and helium. The absorbed fraction depends on the DM candidate - in the form of the initial energy spectrum from the annihilation event - and on the environment where the annihilation takes place, specifically on the ionized fraction of the ambient gas and on the energy density of CMB photons, important for the Inverse Compton (IC) scatterings.

To model this, we use the Monte Carlo scheme MEDEA2 (for details see Evoli et al. 2012b). Through MEDEA2 we are able to calculate what fraction of the energy released by a single annihilation event goes into: (i) H and He ionizations (ii) excitations (iii) heating. A set of handy fitting formulae that take into account the dependence on z and x_e are then given for the respective quantities $f_{\text{ion}}(x_e, z)$, $f_a(x_e, z)$, $f_h(x_e, z)$.

3.2 CMB constraints

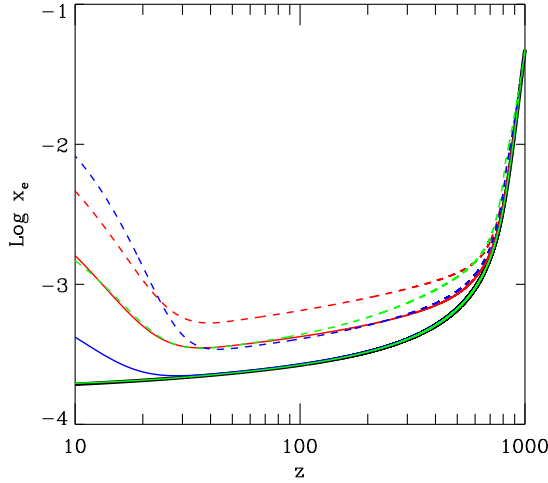
We compute the modifications induced by DM annihilations on the CMB power spectra and on the integrated Thomson optical depth to verify that our models are consistent with WMAP7 observations and to put upper limits on $\langle\sigma v\rangle$ for the considered DM candidates. To do so we modify the public code CAMB (Lewis & Challinor 2011) and add a DM term to the evolution equations of the IGM kinetic temperature and ionized fraction (Fig.1).

With this modified version of CAMB code we can calculate the effects of DM annihilations on the temperature (TT), polarization (EE) and temperature-polarization (TE) CMB spectra. The TT spectrum allows us to put the most sensitive constraints of DM properties (see Fig.2). Our results are obtained assuming that the cosmological parameters have best-fitting values as indicated by the 7-yr WMAP

⁷ Although extrapolating the halo mass function down to such small masses is highly uncertain, we note that at the scales and redshifts of interest, the Press-Schechter and Sheth-Thormen cumulative mass functions (Press & Schechter 1974; Sheth & Tormen 1999; Jenkins et al. 2001) agree to $\sim 10\%$.

Table 1. The DM models described in Sec. 2.

DM model	mass [GeV]	$\langle\sigma v\rangle$ [cm^3/s]	ϵ_0 [eV/s]	$\delta\tau_e$	Line style
W^+W^-	200	$\langle\sigma v\rangle_{th} = 3.0 \times 10^{-26}$	5.35×10^{-25}	1.53×10^{-3}	blue solid
W^+W^-	200	$\langle\sigma v\rangle_{max} = 1.2 \times 10^{-24}$	2.14×10^{-23}	6.09×10^{-2}	blue dashed
$b\bar{b}$	10	$\langle\sigma v\rangle_{th} = 3.0 \times 10^{-26}$	1.07×10^{-23}	1.80×10^{-2}	red solid
$b\bar{b}$	10	$\langle\sigma v\rangle_{max} = 1.0 \times 10^{-25}$	3.57×10^{-23}	5.76×10^{-2}	red dashed
$\mu^+\mu^-$	1000	$\langle\sigma v\rangle_{th} = 3.0 \times 10^{-26}$	1.07×10^{-25}	1.42×10^{-4}	green solid
$\mu^+\mu^-$	1000	$\langle\sigma v\rangle_{max} = 1.4 \times 10^{-23}$	4.99×10^{-23}	6.18×10^{-2}	green dashed

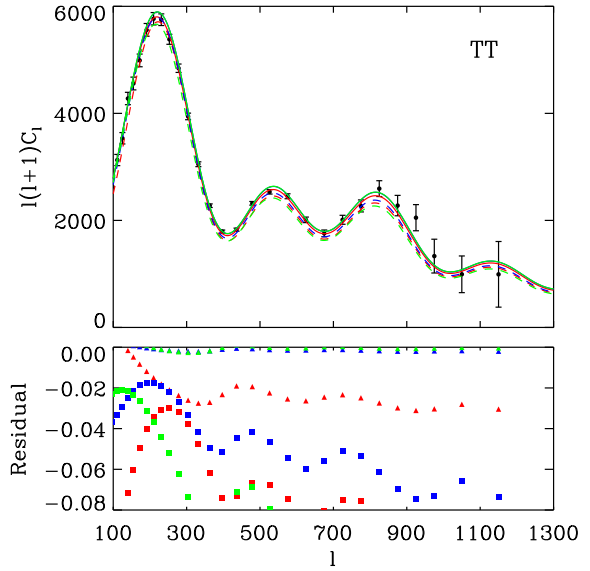
**Figure 1.** IGM ionization fraction as a function of redshift. Black solid line is the case without annihilating DM, for the color scheme of the DM models see Tab. 1.

data (Komatsu et al. 2011). For each DM candidate we increase the value of the thermally averaged annihilation cross section from the standard value $\langle\sigma v\rangle_{th} = 3 \times 10^{-26} \text{cm}^3 \text{s}^{-1}$ up to a value $\langle\sigma v\rangle_{max}$ for which the computed TT CMB spectrum exceeds by more than 3σ from the best-fit the WMAP7 data. The upper limits $\langle\sigma v\rangle_{max}$ for each of the considered DM candidates are given in Tab. 1 along with the color and line-style later used in the plots. CMB observations by Planck will allow to put more stringent constraints on the properties of the DM candidates in the near future (The Planck Collaboration 2006; Galli et al. 2009).

We then calculate the contribution of DM to the Thomson optical depth, $\delta\tau_e$, by integration:

$$\delta\tau_e = \int_6^{10^3} c\sigma_T \delta x_e(z) N_b(z) \left| \frac{dz}{dz} \right| dz \quad (4)$$

where δx_e is the difference in the ionized fraction between the standard scenario and the case in which DM annihilates. We assume here that the Universe is fully ionized at redshift $z < 6$: this contributes by a factor $\tau_e \approx 0.04$ to the WMAP measured total optical depth $\tau_e = 0.088 \pm 0.015$ (Komatsu et al. 2011; Shull et al. 2012). Note that DM annihilations are only imprinted on the CMB as an additional source of ionization. Therefore the above procedure is effectively the same as choosing an upper limit for the extra contribution to τ_e from DM annihilations. From Tab. 1 we see that this is $\delta\tau_e \approx 0.06$, making the total optical depth

**Figure 2.** (Top panel) TT CMB power-spectrum for the DM models in Tab. 1. Black solid line is the case without annihilating DM. (Bottom) Residual of the CMB power-spectrum with respect to the case without DM annihilations. The DM models are presented in red (10 GeV); blue (200 GeV); green (1 TeV). The triangles and squares are used for $\langle\sigma v\rangle_{th}$ and $\langle\sigma v\rangle_{max}$ respectively.

(in the absence of any additional astrophysical sources at $z > 6$): $\tau_e \approx 0.1$. This limit is conservatively low, roughly corresponding to the $1\text{-}\sigma$ upper limit from WMAP7 obtained from the TE cross-correlation (Komatsu et al. 2011).

Notice that the heating/ionization contribution of the two heavier DM candidates assuming $\langle\sigma v\rangle_{max}$ increases proportionally by a larger factor over the case with $\langle\sigma v\rangle_{th}$ than what found for the 10 GeV Bino when assuming $\langle\sigma v\rangle_{max}$ rather than $\langle\sigma v\rangle_{th}$. This is due to our assumption of a smaller minimum halo mass $M_{\min} = 10^{-9} M_\odot$ that enhances strongly the effects of substructures and to which the CMB constraints are, on the other hand, less sensitive.

3.3 21 cm signal

One of the observable quantities most likely to carry a trace of the effects of DM annihilations is the redshifted 21 cm line associated with the hyperfine transition between the triplet and the singlet levels of the neutral hydrogen ground state. This signal is most commonly expressed in terms of the differential brightness temperature between a neutral hydrogen

patch and the CMB (neglecting redshift-space distortions):

$$\begin{aligned} \delta T_b = & \frac{T_S - T_{\text{CMB}}}{1+z} (1 - e^{-\tau}) \approx \\ & 27 x_{\text{HI}} (1 + \delta) \left(1 - \frac{T_{\text{CMB}}}{T_S} \right) \\ & \times \left(\frac{1+z}{10} \frac{0.15}{\Omega_M h^2} \right)^{1/2} \left(\frac{\Omega_b h^2}{0.023} \right) \text{mK}, \end{aligned} \quad (5)$$

where x_{HI} is the neutral fraction of the gas, δ the overdensity, and T_S is the spin temperature which is set by the number densities of hydrogen atoms in the singlet (n_0) and triplet (n_1) ground hyperfine levels, $n_1/n_0 = 3 \exp(-0.068 \text{K}/T_S)$.

It is theoretically well known that in the presence of the CMB alone, T_S reaches thermal equilibrium with $T_{\text{CMB}} = 2.73(1+z)$ K on a short time-scale, making the HI undetectable in emission or absorption. However, collisions and scattering of Ly α photons – the so-called Wouthuysen-Field process or Ly α pumping (e.g. Wouthuysen 1952; Field 1959; Hirata 2006) can couple T_S to T_K .

The spin temperature can be written as (e.g. Furlanetto, Oh & Briggs 2006):

$$T_S^{-1} = \frac{T_{\text{CMB}}^{-1} + x_\alpha T_\alpha^{-1} + x_c T_K^{-1}}{1 + x_\alpha + x_c} \quad (6)$$

where T_α is the color temperature, which is closely coupled to T_K (Field 1959), and x_α and x_c are the two coupling coefficients relative to Ly α scattering and collisions respectively. If either collisions or Ly α radiation couple T_S to T_K then the neutral hydrogen will be visible in absorption or emission depending on whether the gas is colder or hotter than the CMB respectively.

For details about the physics associated with the HI 21 cm line and with the determination of T_S , the quantity that governs it, we refer the reader to, e.g., Furlanetto, Oh & Briggs (2006); Hirata (2006); Valdés & Ferrara (2008). For our purposes it is important to state here that the physical quantities that determine T_S are: (i) the gas density n_H ; (ii) the CMB temperature T_{CMB} ; (iii) the kinetic temperature of the gas, T_K ; (iv) the ionized fraction x_e ; and (v) the Ly α background intensity J_α .

While we know the average evolution of n_H and T_{CMB} we have to determine the others as a function of redshift. The equations that describe the average evolution of the ionized fraction x_e and of the kinetic temperature T_K are the following (see e.g. Chen & Kamionkowski 2004; Mesinger, Furlanetto & Cen 2011):

$$\frac{dx_e}{dz} = \frac{dt}{dz} [\Gamma_{\text{ion}} - \alpha_B x_e^2 n_b f_H] , \quad (7)$$

$$\frac{dT_K}{dz} = \frac{2T_K}{1+z} + \frac{2}{3k_B(1+f_{\text{He}}+x_e)} \frac{dt}{dz} \sum_p \epsilon_p ,$$

where $n_b = n_{b,0}(1+z)^3$ is the mean baryon number density, $\epsilon_p(z)$ is the heating rate per baryon for each process p in erg s^{-1} , Γ_{ion} is the ionization rate per baryon, α_B is the case-B recombination coefficient, k_B is the Boltzmann constant and f_{He} is the helium fraction by mass.

The term Γ_{ion} includes both the contribution from galaxies and the term that accounts for DM annihilations. Similarly we have that $\epsilon_p(z) = \epsilon_{\text{CMB}}(z) + \epsilon_X(z) + \epsilon_{\text{DM}}(z)$ is

the sum of three contributions: (i) $\epsilon_{\text{CMB}}(z)$ is Compton heating from CMB photons; (ii) $\epsilon_X(z)$ is heating from astrophysical sources, which we take to be dominated by X-rays; (iii) $\epsilon_{\text{DM}}(z)$ is DM heating. Notice that when including DM in the terms Γ_{ion} and $\epsilon_p(z)$ we use the specific fractional energy depositions $f_h(x_e, z)$, $f_{\text{ion}}(x_e, z)$ from Evoli et al. (2012b).

The last equation needed to compute the 21 cm background is the one describing the evolution of the Ly α background intensity J_α :

$$J_\alpha = J_{\alpha,R} + J_{\alpha,C} + J_{\alpha,*} + J_{\alpha,X} + J_{\alpha,DM}, \quad (8)$$

where the contributions on the RHS correspond to recombinations, collisional excitations by electron impacts, direct stellar emission, X-ray excitation of HI, and DM annihilations (respectively) (see e.g. Madau, Meiksin & Rees 1997; Valdés et al. 2007; Mesinger, Furlanetto & Cen 2011). The coupling coefficient, x_α is proportional to the Lyman α background flux, J_α (e.g. Furlanetto, Oh & Briggs 2006).

In general, if we neglect the energy input from DM, we expect T_K and T_S to track T_{CMB} down to $z \sim 300$, when T_K decouples from T_{CMB} and starts decreasing adiabatically as the Universe expands. T_S is then coupled to T_K due to the high gas density and the consequent strong collisional coupling. At $z \sim 70$ T_S gradually couples to T_{CMB} until, at $z \sim 30$ becoming virtually identical to it. It is believed however that at around this redshift the first collapsed luminous sources would ignite. Radiation produced by the first galaxies starts to ionize and heat the gas: on a short timescale, at a redshift $z_{\text{WF}} \sim 25 - 30$, the Ly α pumping effectively couples T_S to T_K , and only later, at $z_{\text{heat}} \sim 18 - 22$, heating from galaxies drives T_K to values higher than T_{CMB} , making the neutral regions in the IGM visible in emission. Therefore a second absorption feature is expected at $z_{\text{heat}} \lesssim z \lesssim z_{\text{WF}}$ (see e.g. Furlanetto, Oh & Briggs 2006; Pritchard & Loeb 2008). We can divide the global evolution of δT_b in six main phases:

- (i) $\delta T_b = 0$ for $z \gtrsim 300$;
- (ii) $\delta T_b < 0$ for $30 \lesssim z \lesssim 300$: this extended absorption feature has a minimum of ~ 45 mK at $z \sim 90$;
- (iii) $\delta T_b \sim 0$ for $z_{\text{WF}} \lesssim z \lesssim 30$;
- (iv) $\delta T_b < 0$ at $z_{\text{heat}} \lesssim z \lesssim z_{\text{WF}}$, a second absorption feature less extended in redshift than the previous one but deeper, with $\delta T_{b,\text{min}} \sim -150$ mK;
- (v) $\delta T_b > 0$, i.e. in emission, due to heating by galaxies at $z \lesssim z_{\text{heat}}$ down to the Epoch of Reionization at $z = z_{\text{EoR}} \sim 6 - 8$;
- (vi) $\delta T_b \sim 0$ for $0 \lesssim z \lesssim z_{\text{EoR}}$, where we still have a signal only from self-shielded systems.

Introducing the effects of DM annihilations in the standard scenario described above can produce deviations on δT_b : in particular the second absorption feature can be strongly modified by energy release by DM annihilations, at a redshift range $15 \lesssim z \lesssim 25$ that will be probed by the next generation of radio observatories such as LEDA and SKA.

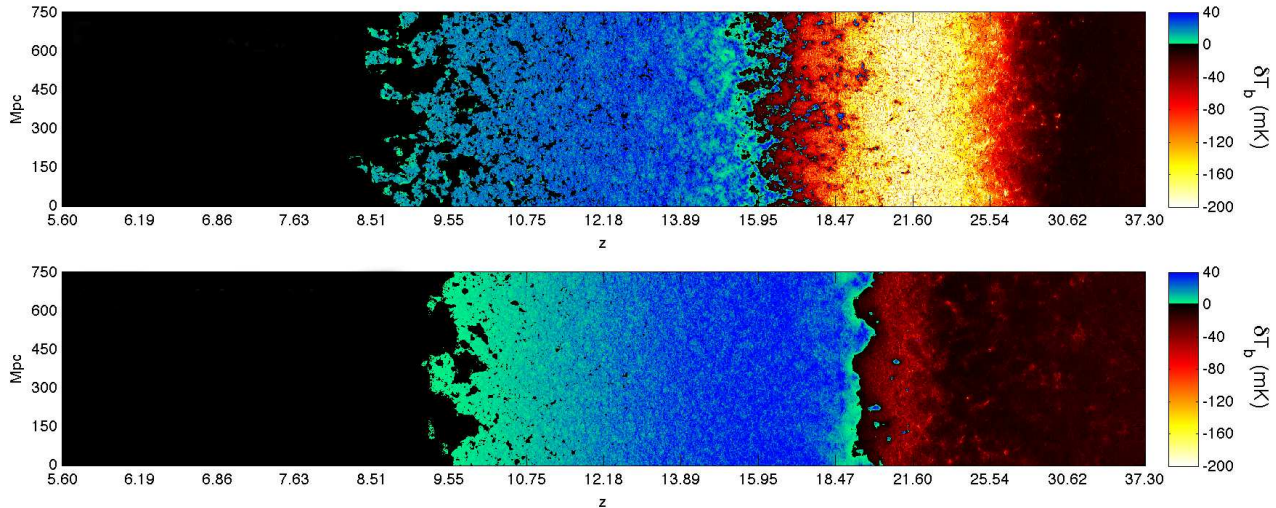


Figure 3. Slices through the 21cm brightness temperature maps for two models with different prescriptions for the galaxy properties (Mesinger, Ferrara & Spiegel 2012). The simulations are 750 Mpc on a side, with a resolution of 500^3 . Each slice is 1 cell (1.5 Mpc) thick. The horizontal axis shows evolution along the comoving line-of-sight coordinate. The top panel corresponds to a “fiducial” model, in which the X-ray luminosity of primordial galaxies is the same as that observed in nearby starburst galaxies, while the lower panel corresponds to a model in which primordial galaxies are much more efficient in generating X-rays, saturating the soft X-ray background at $z \gtrsim 10$ (see text for details).

3.4 Radiation from astrophysical sources

To compute the astrophysical contribution to Γ_{ion} , ϵ_p , and J_α , we use the publicly available code, 21cmFAST⁸. This code uses a combination of perturbation theory and excursion-set formalism to compute various cosmic fields, and is in good agreement with radiative transfer simulations of reionization (e.g. Mesinger & Furlanetto 2007; Zahn et al. 2011; Mesinger, Furlanetto & Cen 2011). The code is fully described in Mesinger, Furlanetto & Cen (2011), to which we refer the interested reader for more details. Here we briefly note that the code takes into account inhomogeneous X-ray ionization and heating, as well as Ly α pumping from the first UV sources, integrating the evolution of cosmic structures and radiation fields along the light cone. Although 21cmFAST computes 3D realizations, in this work we only study the global 21cm signal, deferring analysis of the spatial structure to future work.

The simulation boxes are 750 Mpc on a side, with a final resolution of 500^3 . The initial conditions are sampled on a 1500^3 grid. In Fig. 3 are presented the 1-cell thick (1.5 Mpc deep) slices through the HI 21 cm brightness temperature maps for two models with different prescriptions for the galaxy properties (Mesinger, Ferrara & Spiegel 2012). The top panel corresponds to a “fiducial”⁹ model, in which the X-ray luminosity of primordial galaxies is the same as

that observed in nearby starburst galaxies (e.g. Furlanetto 2006 and references therein). The lower panel corresponds to an “extreme” model in which primordial galaxies, albeit rarer and appearing later, were much more efficient in generating hard X-rays. The later scenario is inspired by recent theoretical (e.g. Linden, Profumo & Anderson 2010; Mirabel et al. 2011) and observational (Reichardt et al. 2011; Mesinger, McQuinn & Spergel 2012) claims. More specifically, these two models have the following characteristics:

(i) *fiducial* (top panel): Galaxies hosting UV and X-ray sources reside in atomically-cooled halos with virial temperatures $T_{\text{vir}} > 10^4$ K (corresponding to halo masses of $M_{\text{halo}} > 3 \times 10^7 M_\odot$ at $z \approx 20$). Ly α pumping (i.e. spin temperature coupling) is dominated by early UV sources, assuming PopII stellar spectra (e.g. Barkana & Loeb 2005) and a 10% efficiency of conversion of gas into stars. The X-ray luminosity of galaxies follows a $h\nu^{-1.5}$ power law shape with a lower limit of $h\nu_0 = 300$ eV (e.g. Madau et al. 2004), and an X-ray efficiency corresponding to ~ 2 X-ray photons per stellar baryon. Similar models, inspired by lower-redshift X-ray binary-dominated star-burst galaxies, have been explored in prior analytic studies (e.g. Furlanetto 2006; Pritchard & Furlanetto 2007).

(ii) *extreme* (bottom panel): Galaxies hosting UV and X-ray sources reside in more massive halos, similar to ones observed at moderate redshifts (e.g. Labbe et al. 2010) and which are more resilient to feedback effects (e.g. Springel & Hernquist 2003; Mesinger & Dijkstra 2008; Okamoto, Gao & Theuns 2008). These galaxies have virial temperatures $T_{\text{vir}} > 10^5$ K, corresponding to halo masses of $M_{\text{halo}} > 10^9 M_\odot$ at $z \approx 20$. Interestingly, in this case Ly α pumping is dominated by the X-ray excitation of HI, and has a very different spatial signature from the fidu-

⁸ <http://homepage.sns.it/mesinger/Sim.html>

⁹ Notice that our “fiducial” model does not exactly correspond to the fiducial model in Mesinger, Ferrara & Spiegel 2012 (consistent with the recent measurement of the 0.5 – 8 keV X-ray luminosity of star forming galaxies from Mineo, Gilfanov & Sunyaev 2012), but instead corresponds to their T1e4_fuv1.fx5_1keV model (based on an extrapolation of the 2 – 10 keV data from Gilfanov, Grimm & Sunyaev 2004). This model represents a more conservative choice since the astrophysical heating is 4 times higher, thus making the DM annihilation signal less apparent.

cial model. The X-ray luminosity of galaxies also follows a $h\nu^{-1.5}$ power law shape, but with a more energetic lower limit of $h\nu_0 = 900$ eV (corresponding to heavy obscuration, e.g. [Lutovinov et al. 2005](#)), and an X-ray efficiency corresponding to ~ 4000 X-ray photons per stellar baryon. This scenario is considered “extreme” since the $z \gtrsim 10$ X-ray sources dominate reionization and saturate the unresolved soft X-ray background ([Hickox & Markevitch 2007](#); [Mesinger, Ferrara & Spiegel 2012](#)).

Both scenarios are consistent with the WMAP7 constraints on τ_e at 2σ ([Komatsu et al. 2011](#)). Notice that the values of $\langle\sigma v\rangle_{max}$ computed in Section 3.2 represent an upper limit and are not self-consistent with the contribution to τ_e from the astrophysical sources modelled by 21cmFAST. On the other hand the DM models with the thermal cross-section $\langle\sigma v\rangle_{th}$ are fully consistent since they only contribute negligibly to τ_e .

It is obvious from Fig. 3 that the fundamental epochs in cosmic evolution show very different 21cm signatures in the two models: spin temperature (WF) coupling (black \rightarrow yellow); X-ray heating of the IGM (yellow \rightarrow blue); reionization (blue \rightarrow black). Here we focus on the global HI 21 cm signal as a way to constrain DM and save spatial signature for future work.

4 RESULTS

We present here the results obtained for the three DM models introduced in Sec. 2, each with two values for the annihilation cross $\langle\sigma v\rangle$: the standard thermal value, and the maximum allowed by CMB constraints as described in Sec 3.2. We solve the evolution equations of the kinetic temperature and ionized fraction of the IGM for each of these DM candidates using the fractional energy depositions from the code MEDEA2 and use a prescription for the formation of collapsed sources of radiation from the publicly available code 21cmFAST, that allows us to include consistently X-ray heating, ionization and Ly α pumping from galaxies.

In Fig. 4 we compare the effects produced on T_S by our annihilating DM candidates. To keep the figure simple we don’t plot the modified T_K curves, corresponding to the annihilating DM cases. However the behavior is simple: the kinetic temperature at high redshift increases because of the high density of DM and the corresponding higher chance of annihilations. As the Universe expands and its content is diluted T_K simply settles on a slightly higher adiabat. When the Ly α pumping becomes efficient at $z \lesssim z_{WF}$, then T_S perfectly tracks T_K , which increases sharply at $z \lesssim z_{heat}$.

The additional heating from annihilating DM particles drives T_S closer to T_{CMB} for $40 < z < 100$. Therefore we can expect a reduction of the absorption feature of the homogeneous 21 cm background in that redshift range. A larger thermally averaged cross-section corresponds to stronger effects on T_S for an annihilating DM candidate of a given mass. At the same time, heavier DM candidates deposit their energy into the IGM less efficiently (see [Evoli et al. 2012b](#)), therefore given a certain value of $\langle\sigma v\rangle$ the lower mass DM candidate will generally produce larger deviations on T_S . The effects are much more evident at $z \lesssim 30$: galaxies start to form and quickly drive J_α to values high enough for efficient Ly α pumping. As a consequence T_S decreases sharply

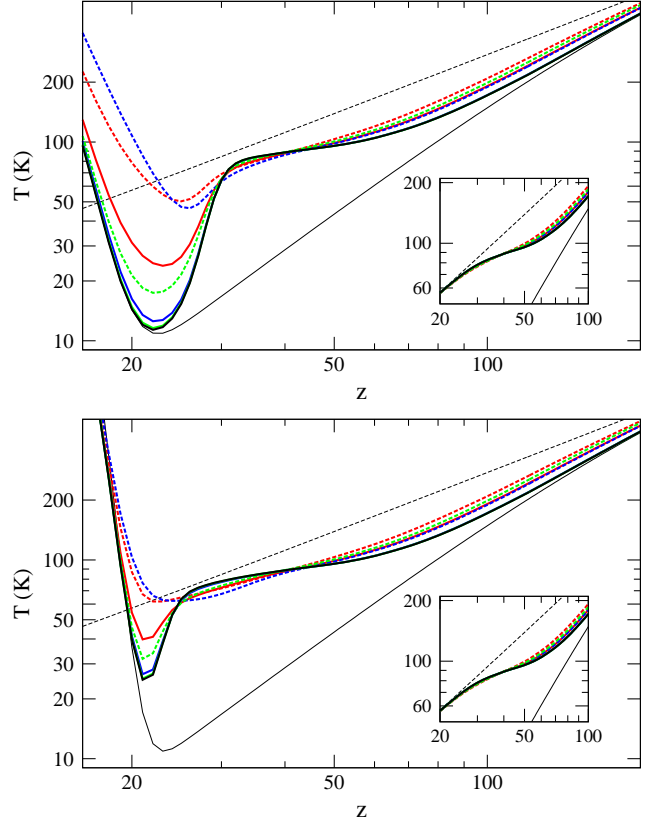


Figure 4. T_S , T_K (thin black solid line) and T_{CMB} (black short-dashed line) as a function of redshift. The colored T_S curves show the modified behavior due to DM annihilations following the color scheme given in Tab. 1. The solid thick black line is the standard T_S without DM energy input. The top and bottom panels represent the calculations done for the *fiducial* and *extreme* models respectively. The box on the lower right corner in each panel shows the behavior of T_S for the considered DM candidates without including radiation from luminous sources.

tracking T_K at a time when the combined heating from DM annihilations and from galaxies is still not sufficient to heat the gas above T_{CMB} . Eventually the same heating sources make $T_K \sim T_S > T_{CMB}$. The different models in the upper and lower panels of Fig. 4 show different behaviors since in the “extreme” case Ly α coupling is achieved later, and the heating starts earlier, making the region at $16 \lesssim z \lesssim 30$ in which $T_S < T_{CMB}$ both shallower (in K) and narrower (in redshift).

This is reflected directly on the behavior of δT_b , shown in the panels of Fig. 5, for which we give a quantitative analysis case by case. A summary of the results is available in Table 2.

4.1 10 GeV Bino

The lightest considered DM candidate, the 10 GeV Bino, produces the largest signature in the “fiducial” model (top panel of Fig. 5), both when assuming a standard thermal cross section $\langle\sigma v\rangle_{th} = 3 \times 10^{-26} \text{cm}^3 \text{s}^{-1}$ (solid red curves in Fig. 5) and when taking into account the maximum cross section allowed by CMB data, in this case $\langle\sigma v\rangle_{max} = 1.0 \times 10^{-25} \text{cm}^3 \text{s}^{-1}$ (dashed red curves). In the

first case the signal is $\delta T_b \sim 4 - 10$ mK on a redshift range $45 \lesssim z \lesssim 300$, with a peak of ~ 10 mK at $z \sim 100$, and is much more substantial for the second absorption feature at $16 \lesssim z \lesssim 30$, with a deviation with respect to the standard case in which DM does not annihilate (which we denote hereafter $\delta T_{b,0}$) of $\Delta T_{b,DM} \equiv |\delta T_b - \delta T_{b,0}| \sim 100$ mK, a large signal at frequencies $\nu \sim 80$ MHz. The effect is enhanced essentially by a factor two for the higher allowed annihilation cross section and reaches values of $\Delta T_{b,DM} \sim 20$ mK at $45 \lesssim z \lesssim 300$, while the second absorption feature at lower redshift is essentially erased, with the IGM appearing in even emission already by $z \lesssim 25$. These very large signals, both for $\langle \sigma v \rangle_{max}$ and for $\langle \sigma v \rangle_{th}$ could be detected by future radio observations (see Section 4.5). In the “extreme” model case (bottom panel) the DM signature before the first astrophysical sources turn on ($z \sim 45 - 300$) is obviously identical to the “fiducial” model case. The second absorption feature instead changes substantially and is both shallower, with a minimum value of $\delta T_b \sim -60$ mK at $z \sim 21$, and narrower in redshift at $z \sim 18 - 25$. This reflects on the DM signal: when assuming $\langle \sigma v \rangle_{th}$ ($\langle \sigma v \rangle_{max}$), $\Delta T_{b,DM} \sim 30$ (45) mK at $z \sim 21$.

4.2 200 GeV Wino

The case of the 200 GeV Wino, described by the blue curves in Fig. 5 produces less evident deviations: assuming $\langle \sigma v \rangle_{th}$ we can see no effect on the δT_b as the solid green line is virtually coincident with the solid black line for both reionization models. Obviously this translates into a constant $\Delta T_{b,DM} = 0$, with no chances of direct detection. On the other hand the case $\langle \sigma v \rangle_{max} = 1.2 \times 10^{-24} \text{ cm}^3 \text{ s}^{-1}$ shows a $\Delta T_{b,DM} = 2 - 9$ mK for $60 \lesssim z \lesssim 300$ and a massive deviation at $z \lesssim 23$ that practically erases the second absorption feature and drives the signal to emission already at $z \sim 20$. This behavior is present for both the fiducial and extreme reionization models.

4.3 1 TeV Leptophilic

Our most massive candidate, the heavy DM particle of rest mass 1 TeV that pair annihilates into leptons, is the one that produces by far the smallest deviations on the HI 21 cm background: for $\langle \sigma v \rangle_{th}$ deviations are negligible while for the maximum allowed cross section, in this case $\langle \sigma v \rangle_{max} = 1.4 \times 10^{-23} \text{ cm}^3 \text{ s}^{-1}$, they reach $\Delta T_{b,DM} \sim 15$ mK in the range $60 \lesssim z \lesssim 300$ and $\Delta T_{b,DM} \sim 65$ (25) mK at $20 \lesssim z \lesssim 30$ for the fiducial (extreme) reionization models.

As mentioned previously, the fractional increase in the DM signal for the two heavier candidates assuming $\langle \sigma v \rangle_{max}$ rather than $\langle \sigma v \rangle_{th}$ is larger than what found for the 10 GeV Bino, due to our choice for the heavier DM particles of a smaller minimum sub-halo mass $M_{\min} = 10^{-9} M_\odot$.

4.4 Isolating the DM annihilation signal

4.4.1 Degeneracy with astrophysics

Although the additional heat input from DM annihilation is easy to isolate in the well-understood epoch of the Dark Ages (before the first astrophysical sources, $z \gtrsim 30 - 50$), the Earth’s ionosphere makes observations of such high redshifts

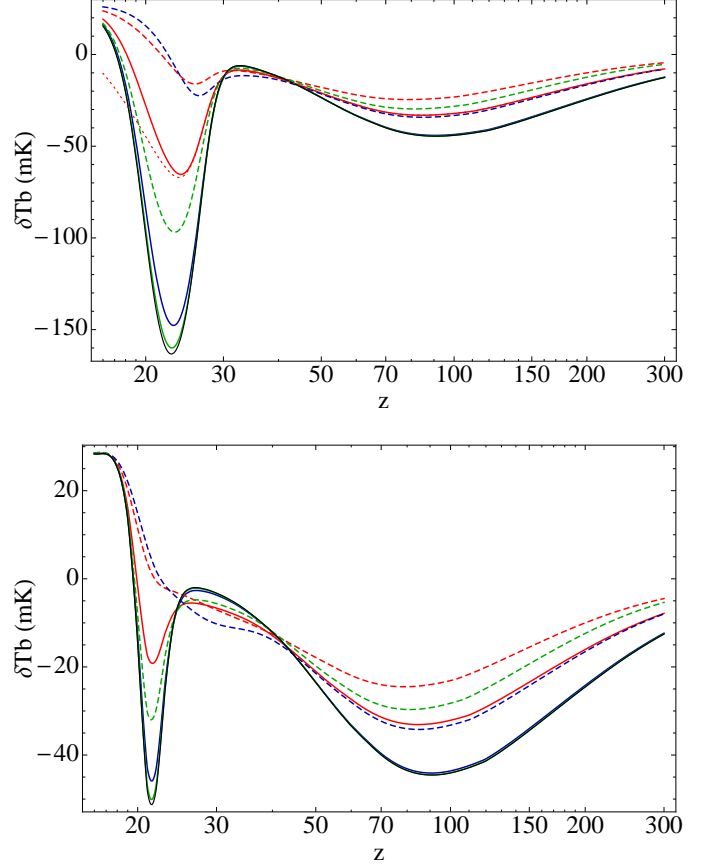


Figure 5. δT_b as a function of redshift for all the considered DM models. The standard case with no energy input from DM annihilations is represented with the thick black line. The colored lines follow the scheme given in Tab. 1. The top and bottom panels represent the calculations done for the *fiducial* and *extreme* models respectively. The red dotted curve in the upper panel corresponds to the thermal Bino model, but ignoring the X-rays from astrophysical sources (i.e. assuming astrophysical sources of X-rays ignited at later times). Notice that some of the curves relative to the DM models are below the black curves at $z = 30 - 40$. This is due to the term $J_{\alpha,DM}$, i.e. the extra Ly α coupling from the DM annihilations.

very challenging (though there are a couple of non-terrestrial radio telescopes being considered, such as DARE and the Lunar Radio Array¹⁰, LRA). The lower-redshift signal at $z_{heat} < z < z_{WF}$ is easier to observe; however in this case the DM annihilation heating must be disentangled from uncertainties in astrophysics. This is evident when comparing the top and bottom panels of Fig. 5. In the “extreme” model in the lower panel the emission from astrophysical sources produces a much shallower absorption feature, and the black solid line could be confused with the red solid line (corresponding to the case of 10 GeV Bino annihilations with $\langle \sigma v \rangle_{th}$) in the upper panel. Therefore detecting a ~ -50 mK global absorption signal at $z \sim 22$ could be an indication of 10 GeV DM annihilations or of a strong X-ray emission by primordial galaxies. Notice however that the

¹⁰ <http://lunar.colorado.edu/lowfreq/>

X-ray emission can be constrained in several ways, e.g. by tighter constraints on the unresolved soft X-ray background of or by a study of the topology of the HII regions once the future radio interferometers start probing the tomography of the IGM beyond the EoR. Unfortunately, both of these observations are only indirect. The soft X-ray background at $z = 0$ only constrains the high-energy component of the source's spectrum ($\sim 20\text{--}40$ keV at $z \sim 20$), which does not interact with the IGM (e.g. McQuinn 2012). Likewise, the EoR at $z \sim 10$ could probe a different source population than was present at $z \sim 20$ (e.g. Ricotti & Ostriker 2004). Nonetheless, if an upper limit is given to the efficiency of the X-ray emission by primordial galaxies a strong reduction of the depth of the absorption feature would be a clear indication of DM annihilations.

4.4.2 DM signal gradient

It is interesting to notice that purely by coincidence galaxies and DM annihilations start to heat the IGM at about the same redshift in these models even though the processes are entirely different and driven by structures with different mass. As previously mentioned, galaxies with mass $M_{\text{halo}} \sim 3 \times 10^7 M_{\odot}$ ($10^9 M_{\odot}$) are responsible for most of the astrophysical X-ray heating at $z = 20$ for the "fiducial" ("extreme") reionization model. On the other hand the function $F(M, z)$ in Eq. 3 peaks strongly for substructures $M_{\text{sh}} \sim 1 M_{\odot}$ at the same redshift, as we show in Fig. 7. The difference in the collapsed fraction above these disparate mass scales is made up by the coefficients in the heating rates. In Fig. 6 we present the heating rates per baryon for 10 GeV DM annihilations (ϵ_{DM}) and for galactic X-ray heating (ϵ_{X}) for the fiducial reionization model, compared with the adiabatic cooling rate (see Eq. 7). Notice that the heating rate from astrophysical sources of X-rays is much steeper than the DM heating, but they become dominant over the adiabatic cooling at about the same redshift. We also plot the heating rate relative to 200 GeV DM annihilations to show that the slope is similar for different DM candidates.

These differences in the slope are easy to understand: the fractional increase of the collapsed fraction in $\gtrsim 1 M_{\odot}$ halos which drive the DM heating is much slower than the fractional increase in the high-end tail of the mass function (i.e. the halos which host the first galaxies). This difference is fundamental, and presents an unambiguous way of disentangling heating from astrophysics and heating from DM.

We quantify this further with the dotted red line in the upper panel of Fig. 5. This curve corresponds to the case of annihilating 10 GeV Binors with $\langle\sigma v\rangle_{th}$, keeping the Ly α pumping due to stellar sources but switching-off astrophysical X-ray heating, which could indeed take place at lower redshifts. The increase of δT_b at $z \lesssim 22$ ($\nu \sim 60$ MHz) here is only due to heating from DM annihilations: the different slope could be a clear indication of DM heating.

In the bottom panel of Fig. 8 we further investigate the difference in slope between the DM and galactic heating and compare them with the standard scenario in which DM does not annihilate. We study the gradient of the signal with frequency, i.e. $d\delta T_b/d\nu$ in mK/MHz, for the 10 GeV Bino, assuming the standard thermal annihilation cross and the fiducial reionization model, and keeping (solid line) or

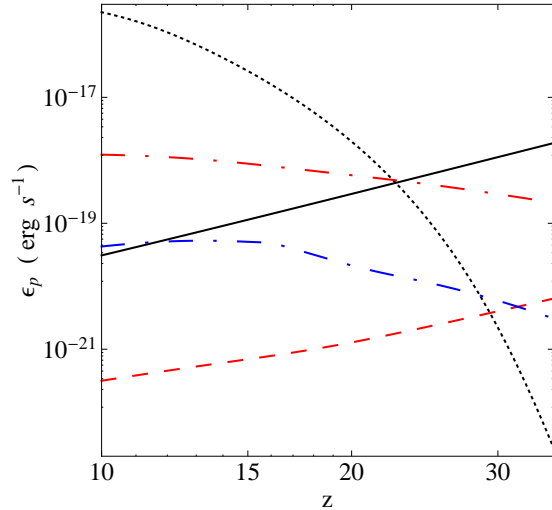


Figure 6. Cooling/heating rates as a function of redshift. We compare here: (i) heating rate $\epsilon_*(z)$ from galaxies for the fiducial reionization model (black dotted line); (ii) $\epsilon_{\text{DM}}(z)$ for 10 GeV DM annihilations assuming a standard $\langle\sigma v\rangle_{th}$ with and without taking into account the boost from substructures (dot-dashed and dashed red lines respectively); (iii) heating from 200 GeV Wino annihilations including the effect of substructures and assuming $\langle\sigma v\rangle_{th}$ (dot-dashed blue line); (iiii) the adiabatic cooling rate of the expanding gas (solid line). Compton heating is negligible at these redshifts. By coincidence heating from 10 GeV DM annihilations and from galaxies becomes dominant over adiabatic cooling at a similar redshift, $z \sim 20$.

switching off (dotted line) the heating from astrophysical sources. We choose the 10 GeV particle because it is the most promising candidate since it produces a strong signal at $z \sim 20$ with $\langle\sigma v\rangle_{th}$, and we assume the "fiducial" model because in the "extreme" case the X-rays drive the heating and ionization of the IGM and produce with secondary interactions the Ly α flux that couples T_S to T_K , therefore it would be incorrect to keep the Ly α pumping and switch off the heating since they are driven by the same sources.

It is evident from the figure that the inclusion of DM heating confines the slope to $d\delta T_b/d\nu \lesssim 4$ mK/MHz (red curves), whereas without DM heating the slope reaches values of $d\delta T_b/d\nu \sim 14$ mK/MHz. This slope would only increase if rarer (more massive) galaxies drive X-ray heating (such as in the "extreme" model). *The detection of such a small peak gradient ($d\delta T_b/d\nu \approx \text{few mK/MHz}$) could provide clear evidence of DM annihilation.*

Including the effects of star formation in smaller sized mini-halos would not alter things significantly, since the fractional increase of the collapsed fraction in mini-halos is still much steeper than that relative to the $\gtrsim 1 M_{\odot}$ sub-halos responsible for the DM heating. In principle, a scenario in which the star formation efficiency within the halos decreases in time (for instance by feedback mechanisms), could reduce the gradient $d\delta T_b/d\nu$. By arbitrarily adjusting the efficiency with time it is possible to perfectly mimic the slower DM heating, however it is unclear how to physically motivate such a rapidly declining star formation efficiency with time. We will explore this aspect in future work.

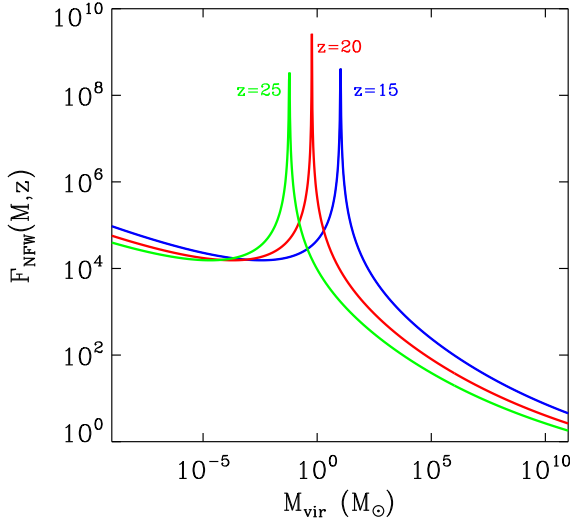


Figure 7. The concentration function adopted to calculate the boost-factor in Eq. 3.

4.5 Observational perspectives

We find that the most promising of our annihilating DM candidates produce a strong deviation in the HI 21 cm line mainly in two redshift ranges: (i) $z \sim 60 - 200$ (corresponding to $\nu \sim 10 - 25$ MHz) with a DM signal $\Delta T_{b,DM} \sim 10 - 20$ mK; (ii) $z \lesssim 18 - 30$ ($\nu \sim 45 - 80$ MHz), where the absorption feature produced by galaxies is strongly suppressed, producing a signal $\Delta T_{b,DM} \sim 20 - 110$ mK depending on the DM particle.

The first high redshift signature is at $\nu \sim 10 - 25$ MHz, a frequency too low to be observed by ground based radio interferometers due to the severe distortions produced by terrestrial ionosphere, which at frequencies $\nu \lesssim 30$ MHz is known to make any observation virtually impossible. Recently a new generation of space or Moon based radio interferometers able to probe the Dark Ages at very low frequencies has been proposed, such as the Dark Ages Lunar Interferometer (DALI, [Lazio et al. 2007](#)), the Lunar Radio Array (LRA, [Lazio et al. 2009](#)) and the Dark Ages Radio Explore (DARE, [Burns et al. 2012](#)). These instruments, if approved and built, would be located on the dark side of the Moon, overcoming two major hurdles of low frequency radio observations, i.e. radio-frequency interference (RFI) from human-generated radio signals, and ionospheric distortions. They could therefore probe the Dark Ages up to $z \sim 100$.

The second signature at $\nu \sim 45 - 80$ MHz could be observed by current or planned radio observatories. We focus here on some of the main experiments.

The LOW Frequency ARray (LOFAR), based in the Netherlands, has two observational bands, a low band (30-85 MHz) and a high band (115-230 MHz). The high band array is the one that will be devoted to the EoR experiment, measuring the redshifted HI 21 cm radiation at $6 \lesssim z \lesssim 11.4$ with a resolution of ~ 3 arcminutes on a field of view of ~ 120 square degrees ([Zaroubi 2012](#)). The low band array probes

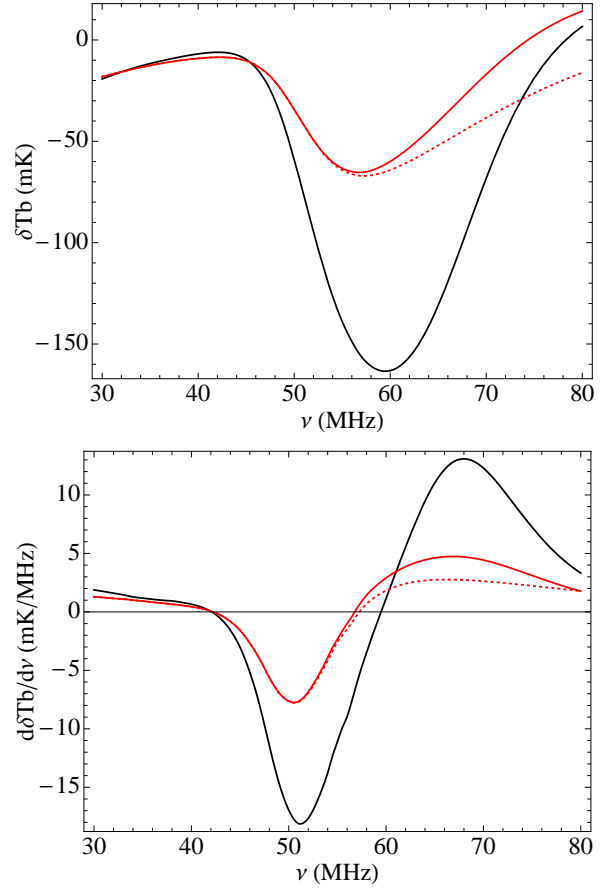


Figure 8. (Top panel) Brightness temperature δT_b as a function of frequency ν assuming the “fiducial” reionization model for three cases: (i) a standard one without DM annihilations (black solid line); (ii) a case including 10 GeV DM annihilations with a standard $\langle \sigma v \rangle_{th}$ and galactic heating and Ly α coupling (red solid line); (iii) a final scenario with 10 GeV DM annihilations with $\langle \sigma v \rangle_{th}$ assuming that galaxies produce Ly α coupling without heating the gas (red dotted line). (Bottom) Gradient $d\delta T_b/d\nu$ of the same quantities. The different slopes relative to heating from DM or galaxies is evident

the frequencies at which the DM signal is stronger, however the detection of HI 21 cm signals at such low frequencies will be beyond reach because of a substantial drop in sensitivity (see e.g. [Zaroubi 2010](#) and references therein).

The Murchison Widefield Array (MWA), located in the radio-quiet Western Australia Outback, will observe at frequencies from 80 to 300 MHz and therefore misses the frequency bands in which a DM signal could be detected.

The Square Kilometer Array (SKA) which is planned to be completed in 2024 in Australia, New Zealand and South Africa, will probe a frequency range from 70 MHz to 10 GHz. The antenna elements that will make up the “SKA-low” array will cover the frequency range $\nu = 70 - 200$ MHz and will achieve a sensitivity an order of magnitude higher than previous experiments. The design is still preliminary and the telescope is at least a decade away from being fully operational, however SKA could detect a DM signal in the HI 21 cm line, if frequencies down to 70 MHz or lower will be probed.

The main scientific goal of the aforementioned inter-

Table 2. DM signal for the considered DM models.

mass [GeV]	$\langle\sigma v\rangle$	model	Peak $\Delta T_{b,DM}$ [mK]
200	$\langle\sigma v\rangle_{th}$	fiducial	15 mK at $z \sim 23$
200	$\langle\sigma v\rangle_{max}$	fiducial	160 mK at $z \sim 23$
200	$\langle\sigma v\rangle_{th}$	extreme	5 mK at $z \sim 21$
200	$\langle\sigma v\rangle_{max}$	extreme	45 mK at $z \sim 21$
10	$\langle\sigma v\rangle_{th}$	fiducial	100 mK at $z \sim 23$
10	$\langle\sigma v\rangle_{max}$	fiducial	160 mK at $z \sim 23$
10	$\langle\sigma v\rangle_{th}$	extreme	30 mK at $z \sim 21$
10	$\langle\sigma v\rangle_{max}$	extreme	45 mK at $z \sim 21$
1000	$\langle\sigma v\rangle_{th}$	fiducial	2 mK at $z \sim 23$
1000	$\langle\sigma v\rangle_{max}$	fiducial	65 mK at $z \sim 23$
1000	$\langle\sigma v\rangle_{th}$	extreme	0.5 mK at $z \sim 21$
1000	$\langle\sigma v\rangle_{max}$	extreme	25 mK at $z \sim 21$

ferometers is however to measure the spatially fluctuating components of the HI 21 cm signal. On the other hand the detection of the angularly averaged all-sky signal could be performed by a single dipole, the main challenge being a precise enough calibration to extract the signal from the backgrounds. This simpler and lower cost alternative is explored by instruments such as EDGES and the Cosmological Reionization Experiment (CoRE, [Chippendale 2009](#)), while more advanced second generation instruments such as the Large-aperture Experiment to Detect the Dark Ages (LEDA) are under construction. A Moon orbiting space observatory such as the Dark Ages Radio Experiment (DARE) seems to be a viable option in the near future, in contrast with the much more complex and expensive task of placing a large interferometer on the dark side of the Moon (DALI, LRA).

The Experiment to Detect the Reionization Step (EDGES) located at the Murchison Radio-astronomy Observatory in Western Australia, measured the radio spectrum between 100 and 200 MHz with all systematic trends in the measurement reduced to below 75 mK, and allowed to exclude a rapid reionization timescale of $\Delta z < 0.06$ at the 95% confidence level. The EDGES team will attempt in the next few years to reduce the systematics of over one order of magnitude and to push observations up to $z \sim 20$ (see e.g. [Bowman & Rogers 2010](#); [McQuinn 2010](#); [Pritchard & Loeb 2010](#)).

One of the most promising instruments for the detection of a DM signal from the Dark Ages is the Large-Aperture Experiment to Detect the Dark Ages (LEDA), a proposed array that will cover a band $\nu \sim 45 - 90$ MHz and that will feature array-based calibration to improve the accuracy of foreground subtraction from the total-power signal ([Greenhill & Bernardi 2012](#)). The fact that LEDA is optimized for the detection of the all-sky HI 21 cm signal together with its low frequency capabilities make it the ideal ground based instrument to detect the HI 21 cm deviations induced by DM annihilations.

5 SUMMARY AND CONCLUSIONS

We consider three of the most popular annihilating DM candidates as sources of X-ray, ionizing and Ly α radiation: thanks to our detailed Monte Carlo treatment MEDEA2 we

computed their energy deposition into the IGM as a function of redshift and ionized fraction. We were then able to calculate precisely and fully consistently the effects of the energy release from DM annihilations on the IGM thermal history and, ultimately, the imprint on the HI 21 cm line at $20 \lesssim z \lesssim 200$. For each DM candidate we compute with a modified version of the publicly available code **CAMB** the deviations produced by each DM model on the CMB power spectrum. This allows us to select two values for the thermally averaged annihilation cross section, the standard thermal case $\langle\sigma v\rangle_{th} = 3 \times 10^{-26} \text{ cm}^3 \text{ s}^{-1}$ and the maximum value $\langle\sigma v\rangle_{max}$ that produces deviations in the CMB power spectrum within 3σ of the WMAP 7 results. We combine each DM model with two prescriptions for radiation from astrophysical sources (computed with the public code **21cmFAST**). We investigate how the formation of luminous sources affects the imprint of DM annihilations on the IGM, and study ways to disentangle the DM signal in this realistic scenario.

Finding a strong deviation in the absorption feature in the all-sky averaged δT_b at $30 \lesssim z \lesssim 200$ will be a clear sign of energy release by DM during a cosmic phase in which no collapsed sources of radiation have yet formed. However it is even more interesting to study the joint effects of energy injection into the IGM from galaxies and DM annihilations at $20 \lesssim z \lesssim 30$, as we find that the Ly α flux from the first luminous sources combined with the early heating from DM annihilations produces strong deviations in the HI 21 cm signal at a redshift range which could be realistically probed by future radio observations in the next few years. Next generation radio facilities such as DALI, LRA or DARE would certainly have ideal characteristics for the detection of a DM signal, but even current or already funded instruments such as MWA, LOFAR and in particular SKA and LEDA would achieve the sensitivity to probe a $\Delta T_{b,DM} \sim 20 - 110$ mK at $\nu \sim 45 - 80$ MHz, if these frequencies will be observed by their final designs and assuming that the strategies for foreground removal and ionospheric corrections will be successful.

We summarize our results as follows.

- *DM annihilation signal.*

(i) Our least massive DM candidate, the 10 GeV Bino like neutralino, produces a large signal in the "fiducial" model, both when assuming the standard thermal cross section $\langle\sigma v\rangle_{th}$ and when taking into account the maximum cross section allowed by CMB data, $\langle\sigma v\rangle_{max}$. In the first case the DM 21 cm signal $\Delta T_{b,DM}$ is of the order of 5 – 10 mK on a redshift range $45 \lesssim z \lesssim 300$ while $\Delta T_{b,DM} \sim 10 - 100$ mK at $20 \lesssim z \lesssim 30$, with the peak signal occurring at a frequency $\nu \sim 80$ MHz. Assuming the higher annihilation cross section $\langle\sigma v\rangle_{max}$ increases $\Delta T_{b,DM}$ and totally erases the second absorption feature at $20 \lesssim z \lesssim 30$, the lack of which represents a very strong - and detectable - DM signature. For the "extreme" reionization model we find in general a smaller signal with a peak $\Delta T_{b,DM} \sim 25$ (50) mK at $z \sim 21$ assuming $\langle\sigma v\rangle_{th}$ ($\langle\sigma v\rangle_{max}$).

(ii) The annihilating 200 GeV Wino produces very different results depending on the $\langle\sigma v\rangle$ assumption of a thermal or maximal value. In the first case $\Delta T_{b,DM}$ is negligible except for a weak signal ~ 15 mK at $z \sim 23$. In the second case instead $\Delta T_{b,DM} \sim 140$ mK at $z \sim 23$ and the second absorption feature driven by Ly α coupling from stars is almost

completely erased. For the extreme case we find a peak signal $\Delta T_{b,DM} \sim 5(45)$ mK at $z \sim 21$ for $\langle\sigma v\rangle_{th}$ ($\langle\sigma v\rangle_{max}$). (iii) The results for our most massive candidate, the heavy DM particle of rest mass 1 TeV that pair annihilates into leptons, are the least promising, with a negligible signal under the assumption of $\langle\sigma v\rangle_{th}$, and a $\Delta T_{b,DM} \sim 60(20)$ mK at $z \sim 23(100)$. For the extreme case we find a peak signal $\Delta T_{b,DM} \sim 0.5(10)$ mK at $z \sim 21$ for $\langle\sigma v\rangle_{th}$ ($\langle\sigma v\rangle_{max}$).

We summarize our results in Table 2.

• *Strategies to isolate the DM signal.*

We find that some of our results for a specific DM model working in the framework of the “fiducial” reionization model (e.g. the case of 10 GeV annihilations assuming $\langle\sigma v\rangle_{th}$) are hard to distinguish from the standard signal $\delta T_{b,0}$ assuming the “extreme” reionization history. However when we study the heating rates per baryon for 10 GeV DM annihilations (ϵ_{DM}) and for galactic X-ray heating (ϵ_X) we notice that the heating rate from astrophysical sources of X-rays evolves much quicker than the DM heating, since the fractional increase of the collapsed fraction in $\gtrsim 1M_\odot$ halos which drive the DM heating is much slower than the fractional increase of the halos which host the first galaxies. This crucial difference presents us with a clean way of disentangling heating by DM annihilations from heating by galaxies. To better quantify this point we study the case of annihilating 10 GeV Binors with $\langle\sigma v\rangle_{th}$, keeping the Ly α pumping due to stellar sources but switching-off astrophysical X-ray heating, which could indeed take place at lower redshifts without breaking any current observational constraints. By coincidence δT_b starts increasing at $z \lesssim 22$ ($\nu \sim 60$ MHz), same as the case in which source heating is taken into account, however DM heating happens with a different slope. We therefore study the gradient of the signal as a function of frequency, $d\delta T_b/d\nu$, and find that when neglecting DM heating the slope reaches values of $d\delta T_b/d\nu \sim 14$ mK/MHz, while in the case in which DM annihilations are taken into account the slope is confined to a considerably smaller $d\delta T_b/d\nu \lesssim 4$ mK/MHz. Although it is possible in principle to mimic the slower DM heating by arbitrarily reducing the star formation efficiency with time, it is unclear whether such an “ad-hoc” model could be physically motivated, and we defer this for future analysis. We can therefore conclude that the detection of a small peak gradient ($d\delta T_b/d\nu \approx \text{few mK/MHz}$) will be a strong evidence of DM annihilation, an exciting prospect that could become reality in the next few years thanks to a new generation of radio instruments such as LEDA and DARE, optimized for the detection of the global HI 21 cm signal during the Dark Ages.

ACKNOWLEDGMENTS

We thank J. Chluba and M. Mapelli for their help in using the numerical codes. CE acknowledges a visiting grant from SNS where part of this work has been carried out, and support from the Helmholtz Alliance for Astro-particle Physics funded by the Initiative and Networking Fund of the Helmholtz Association. NY acknowledges the financial support by the Grants-in-Aid for Young Scientists (S) 20674003 by the Japan Society for the Promotion of Science.

REFERENCES

- Aalseth C. E. et al., 2011a, *Physical Review Letters*, 106, 131301
- , 2011b, *Physical Review Letters*, 107, 141301
- Abdo A. A. et al., 2010, *Physical Review Letters*, 104, 101101
- Aprile E. et al., 2011, *Physical Review Letters*, 107, 131302
- Barkana R., Loeb A., 2005, *ApJ*, 626, 1
- Berg M., Edsjö J., Gondolo P., Lundström E., Sjörs S., 2009, *JCAP*, 8, 35
- Bergström L., Edsjö J., Zaharijas G., 2009, *Physical Review Letters*, 103, 031103
- Bernabei R. et al., 2008, *European Physical Journal C*, 56, 333
- , 2010, *European Physical Journal C*, 67, 39
- , 2004, *arXiv:astro-ph/0405282*
- Bertone G., Cerdeño D. G., Fornasa M., Pieri L., Ruiz de Austri R., Trotta R., 2012, *Phys. Rev. D*, 85, 055014
- Bowman J. D., Morales M. F., Hewitt J. N., 2006, *ApJ*, 638, 20
- Bowman J. D., Rogers A. E. E., 2010, *Nature*, 468, 796
- Bringmann T., 2009, *New Journal of Physics*, 11, 105027
- Burns J. O. et al., 2012, *Advances in Space Research*, 49, 433
- CDMS II Collaboration et al., 2010, *Science*, 327, 1619
- Chen C., Takahashi F., Yanagida T. T., 2009, *Physics Letters B*, 673, 255
- Chen X., Kamionkowski M., 2004, *Phys. Rev. D*, 70, 043502
- Chippendale A. P., 2009, PhD thesis, CSIRO Astronomy and Space Science
- Chluba J., 2010, *MNRAS*, 402, 1195
- Ciafaloni P., Comelli D., Riotto A., Sala F., Strumia A., Urbano A., 2011, *JCAP*, 3, 19
- Cirelli M., Franceschini R., Strumia A., 2008, *Nuclear Physics B*, 800, 204
- Cirelli M., Iocco F., Panci P., 2009, *JCAP*, 10, 9
- Cirelli M., Kadastik M., Raidal M., Strumia A., 2009, *Nuclear Physics B*, 813, 1
- di Bernardo G., Evoli C., Gaggero D., Grasso D., Maccione L., Mazziotta M. N., 2011, *Astroparticle Physics*, 34, 528
- Evoli C., Cholis I., Grasso D., Maccione L., Ullio P., 2012a, *Phys. Rev. D*, 85, 123511
- Evoli C., Valdés M., Ferrara A., Yoshida N., 2012b, *MNRAS*, 422, 420
- Field G. B., 1959, *ApJ*, 129, 536
- Finkbeiner D. P., Galli S., Lin T., Slatyer T. R., 2012, *Phys. Rev. D*, 85, 043522
- Furlanetto S. R., 2006, *MNRAS*, 371, 867
- Furlanetto S. R., Oh S. P., Briggs F. H., 2006, *Phys. Rep.*, 433, 181
- Furlanetto S. R., Oh S. P., Pierpaoli E., 2006, *Phys. Rev. D*, 74, 103502
- Galli S., Iocco F., Bertone G., Melchiorri A., 2009, *Phys. Rev. D*, 80, 023505
- , 2011, *Phys. Rev. D*, 84, 027302
- Gilfanov M., Grimm H.-J., Sunyaev R., 2004, *MNRAS*, 347, L57
- Grajek P., Kane G. L., Phalen D. J., Pierce A., Watson S., 2009, *Phys. Rev. D*, 79, 043506
- Greenhill L. J., Bernardi G., 2012, *arXiv:1201.1700*
- Hickox R. C., Markevitch M., 2007, *ApJL*, 661, L117

- Hirata C. M., 2006, MNRAS, 367, 259
- Hooper D., Tait T. M. P., 2009, Phys. Rev. D, 80, 055028
- Jenkins A., Frenk C. S., White S. D. M., Colberg J. M., Cole S., Evrard A. E., Couchman H. M. P., Yoshida N., 2001, MNRAS, 321, 372
- Kane G., Lu R., Watson S., 2009, Physics Letters B, 681, 151
- Kassim N. E., Lazio T. J. W., Ray P. S., Crane P. C., Hicks B. C., Stewart K. P., Cohen A. S., Lane W. M., 2004, P&SS, 52, 1343
- Komatsu E. et al., 2009, ApJS, 180, 330
- , 2011, ApJS, 192, 18
- Labbe I., et al., 2010, ApJL, 708, L26
- Lazio J., Carilli C., Hewitt J., Furlanetto S., Burns J., 2009, in Society of Photo-Optical Instrumentation Engineers (SPIE) Conference Series, Vol. 7436, Society of Photo-Optical Instrumentation Engineers (SPIE) Conference Series
- Lazio T. J. W. et al., 2007, in Bulletin of the American Astronomical Society, Vol. 39, American Astronomical Society Meeting Abstracts
- Lewis A., Challinor A., 2011, in Astrophysics Source Code Library, record ascl:1102.026, p. 2026
- Linden T., Profumo S., Anderson B., 2010, Phys. Rev. D, 82, 063529
- Liu J., Yuan Q., Bi X., Li H., Zhang X., 2010, Phys. Rev. D, 81, 023516
- Lutovinov A., Revnivtsev M., Gilfanov M., Shtykovskiy P., Molkov S., Sunyaev R., 2005, A&A, 444, 821
- Madau P., Meiksin A., Rees M. J., 1997, ApJ, 475, 429
- Madau P., Rees M. J., Volonteri M., Haardt F., Oh S. P., 2004, ApJ, 604, 484
- Mapelli M., Ferrara A., Pierpaoli E., 2006, MNRAS, 369, 1719
- McQuinn M., 2010, in Astronomical Society of the Pacific Conference Series, Vol. 432, New Horizons in Astronomy: Frank N. Bash Symposium 2009, Stanford L. M., Green J. D., Hao L., Mao Y., eds., p. 65
- , 2012, arXiv:1206.1335
- Mesinger A., Dijkstra M., 2008, MNRAS, 390, 1071
- Mesinger A., Ferrara A., Spiegel D. S., 2012, arXiv:1210.7319
- Mesinger A., Furlanetto S., 2007, ApJ, 669, 663
- Mesinger A., Furlanetto S., Cen R., 2011, MNRAS, 411, 955
- Mesinger A., McQuinn M., Spergel D. N., 2012, MNRAS, 422, 1403
- Mineo S., Gilfanov M., Sunyaev R., 2012, MNRAS, 419, 2095
- Mirabel I. F., Dijkstra M., Laurent P., Loeb A., Pritchard J. R., 2011, A&A, 528, A149
- Natarajan A., Schwarz D. J., 2009, Phys. Rev. D, 80, 043529
- Okamoto T., Gao L., Theuns T., 2008, MNRAS, 390, 920
- Peterson J. B., Pen U., Wu X., 2005, in Astronomical Society of the Pacific Conference Series, Vol. 345, From Clark Lake to the Long Wavelength Array: Bill Erickson's Radio Science, Kassim N., Perez M., Junor W., Henning P., eds., p. 441
- Press W. H., Schechter P., 1974, ApJ, 187, 425
- Pritchard J. R., Furlanetto S. R., 2007, MNRAS, 376, 1680
- Pritchard J. R., Loeb A., 2008, Phys. Rev. D, 78, 103511
- , 2010, Phys. Rev. D, 82, 023006
- Profumo S., 2012, Central European Journal of Physics, 10, 1
- Reichardt C. L. et al., 2011, arXiv:1111.0932
- Ricotti M., Ostriker J. P., 2004, MNRAS, 352, 547
- Shchekinov Y. A., Vasiliev E. O., 2007, MNRAS, 379, 1003
- Sheth R. K., Tormen G., 1999, MNRAS, 308, 119
- Shull J. M., Harness A., Trenti M., Smith B. D., 2012, ApJ, 747, 100
- Slatyer T. R., Padmanabhan N., Finkbeiner D. P., 2009, Phys. Rev. D, 80, 043526
- Springel V., Hernquist L., 2003, MNRAS, 339, 312
- The Planck Collaboration, 2006, arXiv:astro-ph/0604069
- Valdés M., Ferrara A., 2008, MNRAS, 387, L8
- Valdés M., Ferrara A., Mapelli M., Ripamonti E., 2007, MNRAS, 377, 245
- van den Aarssen L. G., Bringmann T., Goedecke Y. C., 2012, arXiv:1202.5456
- Wouthuysen S. A., 1952, AJ, 57, 31
- Wyithe J. S. B., Loeb A., Barnes D. G., 2005, ApJ, 634, 715
- Zahn O., Mesinger A., McQuinn M., Trac H., Cen R., Hernquist L. E., 2011, MNRAS, 414, 727
- Zaroubi S., 2010, arXiv:1002.2667
- , 2012, arXiv:1206.0267